

# Reaction kinetics and isotope effect of water formation by the surface reaction of solid H<sub>2</sub>O<sub>2</sub> with H atoms at low temperatures

Yasuhiro Oba,\* Kazuya Osaka, Naoki Watanabe, Takeshi Chigai and Akira Kouchi

Received 26th November 2013, Accepted 17th January 2014

DOI: 10.1039/c3fd00112a

We performed laboratory experiments on the formation of water and its isotopologues by surface reactions of hydrogen peroxide (H<sub>2</sub>O<sub>2</sub>) with hydrogen (H) atoms and their deuterated counterparts (D<sub>2</sub>O<sub>2</sub>, D) at 10–30 K. High-purity H<sub>2</sub>O<sub>2</sub> (>95%) was prepared *in situ* by the codeposition of molecular oxygen and H atoms at relatively high temperatures (45–50 K). We determined that the high-purity H<sub>2</sub>O<sub>2</sub> solid reacts with both H and deuterium (D) atoms at 10–30 K despite the large activation barriers (~2000 K). Moreover, the reaction rate for H atoms is approximately 45 times faster than that for D atoms at 15 K. Thus, the observed large isotope effect indicates that these reactions occurred through quantum tunneling. We propose that the observed HDO/H<sub>2</sub>O ratio in molecular clouds might be a good tool for the estimation of the atomic D/H ratio in those environments.

## Introduction

Water (H<sub>2</sub>O) is the predominant solid constituent of icy layers of submicron-sized interstellar grains. Because of the potential importance of H<sub>2</sub>O for chemical evolution in molecular clouds (MCs), elucidating the formation mechanism of H<sub>2</sub>O in those environments is important. Although H<sub>2</sub>O formation is possible by gas phase reactions at low temperatures,<sup>1</sup> the observed large abundance of H<sub>2</sub>O cannot be explained only by the gas-phase synthesis.<sup>2</sup> Therefore, it is generally accepted that grain-surface reactions are crucial for producing H<sub>2</sub>O in MCs.

Tielens and Hagen<sup>3</sup> proposed that H<sub>2</sub>O formation is initiated by hydrogenation of atomic oxygen (O), molecular oxygen (O<sub>2</sub>), and ozone (O<sub>3</sub>), and is completed by the following reactions:



N19W8, Kita-ku, Sapporo, Hokkaido, Japan. E-mail: oba@lowtem.hokudai.ac.jp; Fax: +81 11 706 7142; Tel: +81 11 706 5477





Since reaction (1) is a radical–radical reaction, it should proceed immediately once reactants encounter each other on the surface. This reaction has been studied experimentally by several groups.<sup>4–7</sup> In contrast to reaction (1), reactions (2) and (3) have large activation barriers (>2000 K) in the gas phase.<sup>8,9</sup> However, despite such a large barrier, these two reactions were proposed to contribute significantly to H<sub>2</sub>O formation in dense MCs.<sup>10</sup> Since reactions having such large barriers do not occur thermally in MCs, reactions (2) and (3) require quantum tunneling. The quantum tunneling rate  $k_q$  is expressed by the following equation, assuming a rectangular activation barrier with a height  $E_a$  and width  $a$ :<sup>11</sup>

$$k_q \approx \nu_0 \exp[-(2a/\hbar)(2mE_a)^{1/2}], \quad (4)$$

where  $\nu_0$  and  $m$  represent the frequency of harmonic motion and the mass of the reaction, respectively. Since temperature is not included in the equation,  $k_q$  does not depend on the reaction temperature. Further details about quantum tunneling reactions have been described elsewhere.<sup>11–14</sup>

We have recently studied reaction (2) experimentally by the codeposition of nonenergetic OH with H<sub>2</sub> and isotopologues such as OD, HD, and D<sub>2</sub> on a substrate and determined that the reactions occur at 10 K.<sup>14</sup> In addition, significant isotope effects were observed, and reactions of OH and OD abstracting a D atom from HD and D<sub>2</sub> were approximately ten times slower than those abstracting an H atom from H<sub>2</sub> and HD. This isotope effect can be explained by the difference in the effective mass of tunneling reactions.<sup>14</sup>

A number of research studies have been conducted on reaction (3). In these previous studies, O<sub>2</sub> was used as an initial reactant rather than hydrogen peroxide (H<sub>2</sub>O<sub>2</sub>), which was produced by the successive hydrogenation of O<sub>2</sub> as follows:



For example, Miyauchi *et al.*<sup>15</sup> exposed solid O<sub>2</sub> layers to H or D atoms at 10 K and determined that (i) the rate of O<sub>2</sub> hydrogenation (reaction (5)) is equal to that of O<sub>2</sub> deuteration, (ii) the rate of reaction (3) is slower than that of reaction (5), and (iii) the rate of reaction (3) is eight times faster than that of the following isotopically substituted reaction (7):



Miyauchi *et al.* considered that the rate difference between reactions (3) and (7) would be due to the isotope effect of quantum tunneling.<sup>15</sup> However, in the O<sub>2</sub> hydrogenation experiments, the formation of both H<sub>2</sub>O<sub>2</sub> and H<sub>2</sub>O occurs in the sample solid. Furthermore, the parent O<sub>2</sub> molecule is IR-inactive. Thus, multi-parameter fittings, which often cause significant errors, are necessary to obtain the rates for reactions (3) and (5). Moreover, recent studies suggested that H<sub>2</sub>O may form by another exothermic reaction in typical experimental conditions for O<sub>2</sub> hydrogenation:<sup>16,17</sup>





In addition to reaction (3), OH is expected to form by the following pathway:



where  $\text{H}_2\text{O}_2^*$  is a reaction intermediate. The reaction of two OH also yields  $\text{H}_2\text{O}_2$  on the surface:



The branching ratio of barrierless reactions (8) to (10) was determined experimentally<sup>17</sup> to be 1 to 4 at 40 K and theoretically<sup>18</sup> to be 1 to 9 on a cold substrate. In any case, reactions (8) and (10) may compete during  $\text{O}_2$  hydrogenation experiments to some extent, making it more difficult to obtain reliable kinetic parameters for reaction (3). In the case of CO hydrogenation experiments, a similar problem occurred because both formaldehyde ( $\text{H}_2\text{CO}$ ) and methanol ( $\text{CH}_3\text{OH}$ ) were produced in a single experiment.<sup>19–23</sup> However, additional experiments using  $\text{H}_2\text{CO}$  as an initial reactant have enabled us to better understand the reaction kinetics and isotope effects of CO and  $\text{H}_2\text{CO}$  hydrogenation.<sup>13,24</sup> Similarly, the use of  $\text{H}_2\text{O}_2$  as an initial reactant is desirable for studying the kinetics and isotope effects of reaction (3). However, because of difficulty in using pure  $\text{H}_2\text{O}_2$ , to date such an experiment has not been performed.

In the present study, we performed experimental studies on the formation of  $\text{H}_2\text{O}$  *via* reaction (3) and its isotope effect using high-purity (>95%) solid  $\text{H}_2\text{O}_2$  and  $\text{D}_2\text{O}_2$ .

## Experimental

### Apparatus and experimental conditions for water formation

All experiments were performed using the Apparatus for SURface Reaction in Astrophysics (ASURA) system. The ASURA primarily comprises a main chamber and an atomic source. An aluminum (Al) substrate was mounted at the center of the main chamber and all reactions were performed on the substrate at 10–30 K. Hydrogen (H) and deuterium (D) atoms were produced by the dissociation of  $\text{H}_2$  and  $\text{D}_2$  molecules, respectively, in a microwave discharge plasma, and were cooled by multiple interactions with the inner wall of the aluminum pipe, which was cooled to 100 K. We confirmed that the formed H and D atoms were well thermalized to the pipe temperature.<sup>25</sup> Further details of the ASURA have been described elsewhere.<sup>25,26</sup>

The fluxes of H and D atoms were not directly measured in the present experimental setup; they were estimated by comparing the effective rates of CO hydrogenation and deuteration with those reported by Hidaka *et al.*,<sup>27</sup> which were obtained under the same experimental conditions. Briefly, amorphous  $\text{H}_2\text{O}$  ice ( $\alpha\text{-H}_2\text{O}$ ) with a thickness of approximately ten monolayers (ML;  $\sim 10^{15}$  molecules  $\text{cm}^{-2}$ ) was produced by vapor deposition on the substrate at 15 K, followed by the deposition of CO with a thickness of  $\sim 0.8$  ML. The column density of  $\text{H}_2\text{O}$  and CO was calculated from the peak area and the previously published band strengths, as described by Hidaka *et al.*<sup>27</sup> The band strengths for the CO stretching of CO and OH



stretching of H<sub>2</sub>O are  $2.0 \times 10^{-16}$  and  $1.1 \times 10^{-17}$  cm molecules<sup>-1</sup>, respectively.<sup>28</sup> The obtained effective rates were 1.4 and 0.21 min<sup>-1</sup> for the hydrogenation and deuteration of CO, respectively (see Results section below for the determination of effective rate constants). These values are a factor of 3.3 and 6.4 larger than the effective rates of CO hydrogenation and deuteration, respectively, compared to those reported by Hidaka *et al.*,<sup>27</sup> whose fluxes of both H and D atoms were  $2.6 \times 10^{14}$  atoms cm<sup>-2</sup> s<sup>-1</sup>. Assuming that the surface density of H and D atoms correlates linearly with their fluxes, the fluxes of H and D atoms in the present study were estimated to be  $8.7 \times 10^{14}$  and  $1.7 \times 10^{15}$  atoms cm<sup>-2</sup> s<sup>-1</sup>, respectively, which corresponds to a D and H atom flux ratio of  $\sim 2$ . The variations in the H and D fluxes are expected to be less than 10% during and between each experiment.

Approximately 1 ML of solid H<sub>2</sub>O<sub>2</sub> or its deuterated counterpart D<sub>2</sub>O<sub>2</sub> was produced on the substrate by the procedures shown in the next section. H<sub>2</sub>O<sub>2</sub> and D<sub>2</sub>O<sub>2</sub> were exposed to H (D) atoms at 10–30 K. Reaction products were monitored *in situ* by a reflection absorption Fourier Transform Infrared (FTIR) spectrometer with a resolution of 4 cm<sup>-1</sup> in the spectral range from 700 to 4000 cm<sup>-1</sup>. The column density of H<sub>2</sub>O<sub>2</sub> and D<sub>2</sub>O<sub>2</sub> was calculated from the peak area and previously published band strengths.<sup>15</sup> The band strengths used were  $2.1 \times 10^{-17}$  and  $1.5 \times 10^{-17}$  cm molecule<sup>-1</sup> for the OH and OD bending bands at 1385 and 1039 cm<sup>-1</sup>, respectively.

Experiments were also performed on an amorphous D<sub>2</sub>O ice (a-D<sub>2</sub>O;  $\sim 30$  ML) vapor-deposited at 10 K. The band strength used was  $1.3 \times 10^{-16}$  cm molecule<sup>-1</sup> for the OD stretching band.<sup>15</sup>

### Preparation of high-purity solid hydrogen peroxide

In previous studies,<sup>29,30</sup> high-purity H<sub>2</sub>O<sub>2</sub> (>97%) has been prepared by distilling commercially available H<sub>2</sub>O<sub>2</sub> solution under vacuum. The distilled H<sub>2</sub>O<sub>2</sub> was introduced into a reaction substrate through a transfer line made with nonreactive materials such as glass to avoid the catalytic decomposition of H<sub>2</sub>O<sub>2</sub> on metal surfaces. However, in a typical apparatus, which comprises a stainless steel chamber and gas lines, it is not easy to obtain pure H<sub>2</sub>O<sub>2</sub> using this procedure without significant modification.

Thus, we produced high-purity solid H<sub>2</sub>O<sub>2</sub> *in situ* by the codeposition of H atoms with O<sub>2</sub> molecules on a substrate at relatively high temperatures. In our previous study, we determined that H<sub>2</sub>O<sub>2</sub>-rich ice tends to form by the O<sub>2</sub>/H codeposition at high temperatures (>30 K) and with an increasing proportion of O<sub>2</sub> relative to H atoms.<sup>31</sup> For example, when O<sub>2</sub> and H were codeposited with an O<sub>2</sub>/H ratio of  $\sim 2 \times 10^{-3}$  at 20 K, the main product was H<sub>2</sub>O with a small amount of H<sub>2</sub>O<sub>2</sub> (H<sub>2</sub>O/H<sub>2</sub>O<sub>2</sub>  $\sim 5$ ). When the same experiment was performed with an O<sub>2</sub>/H ratio of  $\sim 9 \times 10^{-3}$  at 40 K, the main product was H<sub>2</sub>O<sub>2</sub> with  $\sim 15\%$  contamination of H<sub>2</sub>O. We further extended this experiment for the production of solid H<sub>2</sub>O<sub>2</sub> with higher purity suitable for studying the kinetics and the isotope effect of reaction (3). One of the major advantages of this sample preparation method is that it is possible to study the isotope effect of reaction (3) using different isotopes (*i.e.*, H and D), which was not possible in previous studies.<sup>15,32</sup>

Gaseous O<sub>2</sub> was introduced into the main chamber through a capillary plate. From the pressure inside the main chamber, the O<sub>2</sub> flux was estimated to be  $1.0 \times 10^{14}$  molecules cm<sup>-2</sup> s<sup>-1</sup>, which is two to four orders of magnitude larger than



that used by Oba *et al.*<sup>31</sup> The H atoms were codeposited with O<sub>2</sub> onto the substrate at 45–50 K. In the present experiments, pure H<sub>2</sub>O<sub>2</sub> solid and the solid on a-D<sub>2</sub>O were used as reactants. The amount of solid H<sub>2</sub>O<sub>2</sub> was ~1 ML. After the formation of solid H<sub>2</sub>O<sub>2</sub>, the microwave was switched off, the supply of all gases (H<sub>2</sub> and O<sub>2</sub>) was stopped, and the substrate temperature was raised to 70 K to remove residual O<sub>2</sub> from the sample solid. H<sub>2</sub>O contamination in the solid H<sub>2</sub>O<sub>2</sub> was <5%, which was confirmed by the IR spectrum of the product (Figure 1a). We believe that this small amount of contamination does not significantly impact the kinetics of reaction (3). We confirmed this by a temperature-programmed desorption experiment wherein little O<sub>2</sub> remained on the substrate after the sample treatment. The produced H<sub>2</sub>O<sub>2</sub> was then cooled to the desired temperatures (10–30 K) for hydrogenation or deuteration experiments. Moreover, when D atoms were used, high-purity D<sub>2</sub>O<sub>2</sub> was formed (Figure 1b).

## Results

### H<sub>2</sub>O<sub>2</sub> + H and H<sub>2</sub>O<sub>2</sub> + D

Figure 2 shows IR absorption spectra of solid H<sub>2</sub>O<sub>2</sub> (top) and H<sub>2</sub>O (bottom) for comparison and the difference spectra of 1 ML pure solid H<sub>2</sub>O<sub>2</sub> after H atom exposure for up to 10 min at 15 K (middle). In the difference spectra, the peaks below and above the baseline represent decreases of initial reactant and increase of reaction products, respectively. With increasing H atom fluence, the peak intensity for the OH bending of H<sub>2</sub>O<sub>2</sub> at 1385 cm<sup>-1</sup> decreased, and new peaks appeared at 3000–3600, 2850, and 1660 cm<sup>-1</sup>. The peak at 1660 cm<sup>-1</sup> is attributable to the OH bending of H<sub>2</sub>O formed by reaction (3). Based on the peak position of OH stretching bands of solid H<sub>2</sub>O<sub>2</sub> and H<sub>2</sub>O (Figure 2), the H<sub>2</sub>O band at 3000–3600 cm<sup>-1</sup> has a substantial overlap with that of H<sub>2</sub>O<sub>2</sub>, and the peak shape would be attributable to the sum of H<sub>2</sub>O<sub>2</sub> decrease and H<sub>2</sub>O increase. In addition, H<sub>2</sub>O<sub>2</sub> has another strong peak at 2827 cm<sup>-1</sup>, which is often assigned to the  $\nu_2 + \nu_6$  combination band.<sup>33</sup> If the amount of H<sub>2</sub>O<sub>2</sub> decreases after H atom exposure, the intensity of the peak should also decrease. However, a peak was observed slightly above the baseline at 2850 cm<sup>-1</sup> after H atom exposure, unlike other peaks at ~3300 and 1385 cm<sup>-1</sup> (Figure 2). These apparently contradictory observations will be discussed later in the Discussion section. Two small peaks

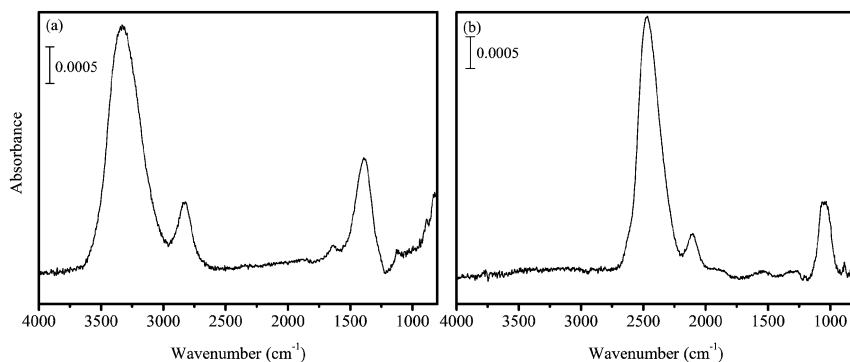


Fig. 1 FTIR spectra of (a) H<sub>2</sub>O<sub>2</sub> and (b) D<sub>2</sub>O<sub>2</sub> produced at 45 K.



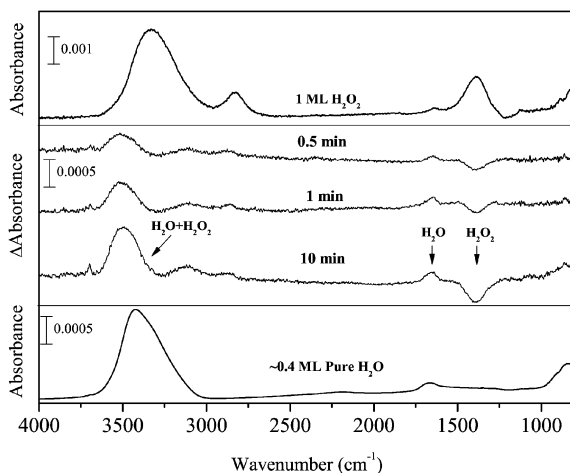


Fig. 2 FTIR spectra of  $\text{H}_2\text{O}_2$  (top) and pure  $\text{H}_2\text{O}$  (bottom) and the variations in the difference spectra of  $\text{H}_2\text{O}_2$  after exposure to H atoms for up to 10 min at 15 K (middle).

appeared at  $3697$  and  $3721\text{ cm}^{-1}$  after H atom exposure (Figure 2), which are attributed to the 3- and 2-coordinated water molecules, respectively.<sup>34</sup>

Figure 3 shows the difference spectra of 1 ML  $\text{H}_2\text{O}_2$  after D atom exposure for up to 120 min at 15 K. If  $\text{H}_2\text{O}_2$  reacts with D atoms, HDO is expected to form as a main product by the following reaction:



After D atom exposure to  $\text{H}_2\text{O}_2$ , the peak area for OH stretching and bending bands decreased. New peaks appeared at  $3490$ ,  $2527$ , and  $1492\text{ cm}^{-1}$ , which are

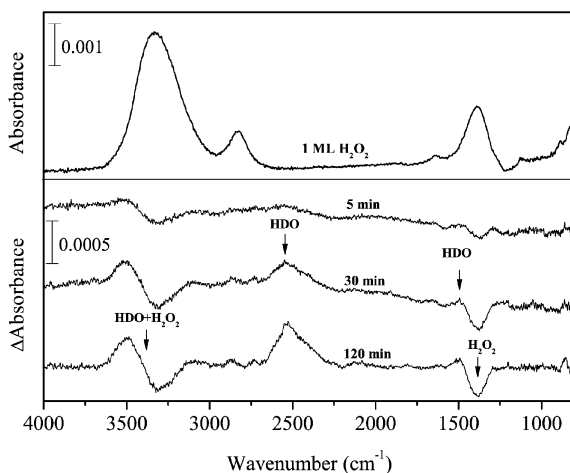


Fig. 3 Variations in the difference spectra of  $\text{H}_2\text{O}_2$  after exposure to D atoms for up to 120 min at 15 K.



typically observed for solid H<sub>2</sub>O at low temperatures.<sup>35,36</sup> This result clearly indicates that HDO was formed by reaction (11) at 15 K. Although the peak area for OH stretching and bending bands decreased after D atom exposure, the  $\nu_2 + \nu_6$  combination band at 2860 cm<sup>-1</sup> increased slightly. Very small peaks appeared at 2722 and 3693 cm<sup>-1</sup> after D atom exposure (Figure 3), the former of which is probably derived from the dangling OD bond of HDO.<sup>37</sup> The latter peak could be the dangling OH bond of HDO; however, the assignment is uncertain because of low S/N.

Figure 4 plots variations in the column density of solid H<sub>2</sub>O<sub>2</sub> normalized to the unexposed initial amount after exposure to H or D atoms. We fitted the plots in Figure 4 to the following single-exponential decay function to obtain the kinetic parameters for reactions (3) and (11):

$$\Delta[\text{H}_2\text{O}_2]/[\text{H}_2\text{O}_2]_0 = A(e^{-k_n[X]t} - 1), \quad (12)$$

where  $A$  is a saturation value,  $t$  is the H or D atom exposure time,  $k_n$  is the rate constant of reaction (n), and  $[X]$  is the number density of X atoms ( $X = \text{H}$  or  $\text{D}$ ) on the surface. Unfortunately, it is difficult to measure  $[X]$  in the present experiment; thus, the product  $k_n[X]$  is obtained as a fitting parameter for equation (12). Hereafter,  $k_n[X]$  is denoted as the effective rate constant  $k_n'$  in the present study. We assume that during exposure,  $[X]$  is independent of time and is governed mainly by the balance between the flux of X atoms, the sticking coefficient of the impinging atoms, and the loss of atoms by X–X recombination. We obtained  $k_3' = 7.2 \times 10^{-1}$  and  $k_{11}' = 3.2 \times 10^{-2} \text{ min}^{-1}$  at 15 K, and the  $k_3'/k_{11}'$  ratio was 23.

In the present study, we do not determine the absolute yields of reaction products with the decrease in the column density of reactants, because the band strengths of the products (H<sub>2</sub>O or HDO) have been reported only for a transmission method. Using these reported values may cause a large error (<50%)<sup>31</sup> when those band strengths are used in a reflection method. However, it does not

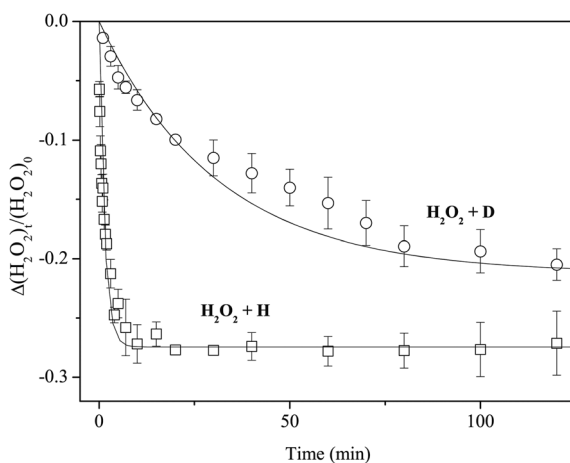


Fig. 4 Variations in the column density of H<sub>2</sub>O<sub>2</sub> normalized to the initial amount as a function of exposure time of H or D atoms at 15 K. Solid lines are single-exponential decay fits to the plots.



affect the values of effective rate constants because the term of band strength is not included in equation (12). In addition, a portion of the reaction products could desorb from the substrate upon formation,<sup>38,39</sup> making the interpretation of the yields of products more difficult.

### $D_2O_2 + H$ and $D_2O_2 + D$

Figure 5 shows variations in the difference spectra of pure solid  $D_2O_2$  after exposure to H atoms on the Al substrate at 15 K. With increasing D atom fluence, the peak intensity of OD stretching and bending bands at 2467 and 1045  $cm^{-1}$ , respectively, decreased, and new peaks appeared at 3455, 2587, and 1477  $cm^{-1}$ . By comparing the peak positions with those given in the literature,<sup>36</sup> we determined that these new peaks are attributable to HDO, indicating that solid  $D_2O_2$  reacted with H atoms to yield HDO at 15 K:



The peak intensity of the  $\nu_2 + \nu_6$  combination band for  $D_2O_2$  (2126  $cm^{-1}$ )<sup>33</sup> increased slightly, which is opposite to the behavior that would be observed if  $D_2O_2$  was consumed by reaction (13). The dangling OH band of HDO was observed at 3694  $cm^{-1}$  while the dangling OD band was not confirmed probably due to low S/N (Figure 5).

Figure 6 shows variations in the difference spectra after D atom exposure to  $D_2O_2$  for up to 120 min at 15 K. This experiment was performed to study reaction (7):



This reaction has been studied in previous  $O_2$  deuteration experiments.<sup>15,32</sup> In the present study, with increasing D atom fluence, new peaks appeared at 2562 and

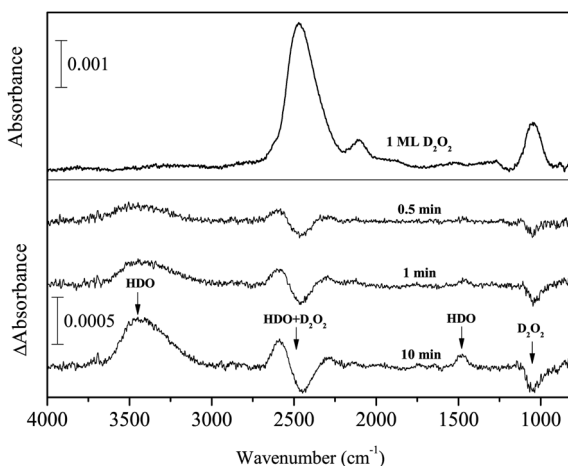


Fig. 5 Variations in the difference spectra of  $D_2O_2$  after exposure to H atoms for up to 10 min at 15 K.



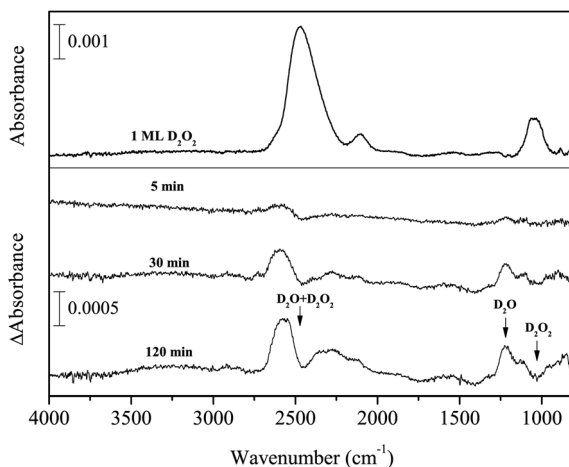


Fig. 6 Variations in the difference spectra of  $D_2O_2$  after exposure to D atoms for up to 120 min at 15 K.

$1220\text{ cm}^{-1}$ , concurrent with the decrease of  $D_2O_2$  (Figure 6). The new peaks can be attributed to the OD stretching and bending of  $D_2O$ , which clearly indicates that reaction (7) occurred to yield  $D_2O$  on the surface at 15 K. A small peak was observed after exposure to D atoms at  $2727\text{ cm}^{-1}$ , which is assigned to the 3-coordinated dangling OD band of  $D_2O$ .<sup>34</sup> A 2-coordinated dangling OD band (at  $2748\text{ cm}^{-1}$ )<sup>34</sup> was not firmly identified, probably due to the low S/N of the spectrum. The peak intensity of the  $\nu_2 + \nu_6$  combination band for  $D_2O_2$  increased as well (Figure 6).

Figure 7 shows variations in the column density of solid  $D_2O_2$  normalized to the unexposed initial amount after H or D atom exposure at 15 K. The relative abundance of  $D_2O_2$  by reaction (13) reaches a saturation value of approximately

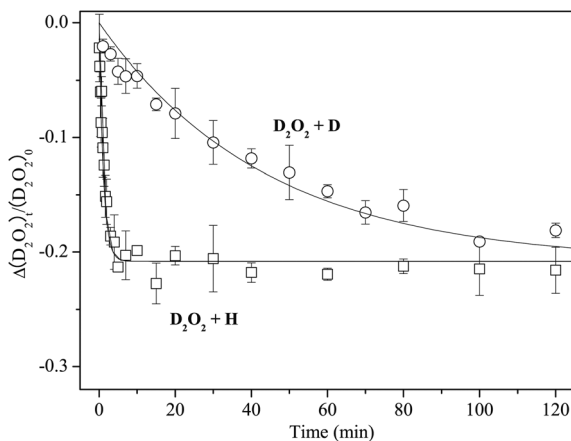


Fig. 7 Variations in the column density of  $D_2O_2$  normalized to the initial amount as a function of H or D atom exposure times at 15 K. Solid lines are single-exponential decay fits to the plots.



–0.2 after a few minutes. In contrast, the decrease of  $D_2O_2$  by reaction (7) was much slower, reaching the almost same saturation value after 150 min. By fitting the plots in Figure 7 into single exponential decay function (12) where  $[H_2O_2]$  is replaced with  $[D_2O_2]$ , we obtained  $k_{13}' = 8.9 \times 10^{-1}$  and  $k_7' = 2.3 \times 10^{-2} \text{ min}^{-1}$ , and the  $k_{13}'/k_7'$  ratio was 38.

### Reactions on amorphous $D_2O$ ice

Hydrogenation and deuteration of solid  $H_2O_2$  and  $D_2O_2$  were also performed on vapor-deposited a- $D_2O$  with a thickness of  $\sim 30$  ML at 15 K. Figure 8 shows an IR spectrum of 1 ML solid  $H_2O_2$  produced on a- $D_2O$  and the difference spectra after H atom exposure for up to 5 min. The peak area of the  $\nu_2 + \nu_6$  combination band before H atom exposure was larger by a factor of two than that on the Al substrate, although the peak area of other bands (OH stretching and bending) was almost equal.

With increasing H atom fluence, the intensities of peaks at 3233, 2852, and  $1392 \text{ cm}^{-1}$  decreased and new peaks appeared at 3422 and  $1635 \text{ cm}^{-1}$ . These observations clearly indicate that  $H_2O$  was formed by reaction (13). Notably, the peak intensity for the  $\nu_2 + \nu_6$  combination band at  $2852 \text{ cm}^{-1}$  decreased after H atom exposure. This behavior is straightforward since  $H_2O_2$  was consumed by reaction (13); however, interestingly, this is opposite to the result for the same reactions of pure  $H_2O_2$  on the Al substrate described above. In addition to reaction (13), we confirmed in separate experiments that reactions (11), (13), and (7) occur on a- $D_2O$  at 15 K. Two small peaks appeared at 3697 and  $3719 \text{ cm}^{-1}$  after exposure to H atoms (Figure 8), which are attributed to the 3- and 2-coordinated dangling OH bands, respectively.<sup>34</sup>

We determined the effective rate constants with statistical errors for each reaction (Table 1) by fitting the attenuation of  $H_2O_2$  and  $D_2O_2$  into a single exponential decay function (12). As a general trend, values of  $k'$  are larger for reactions on a- $D_2O$ .

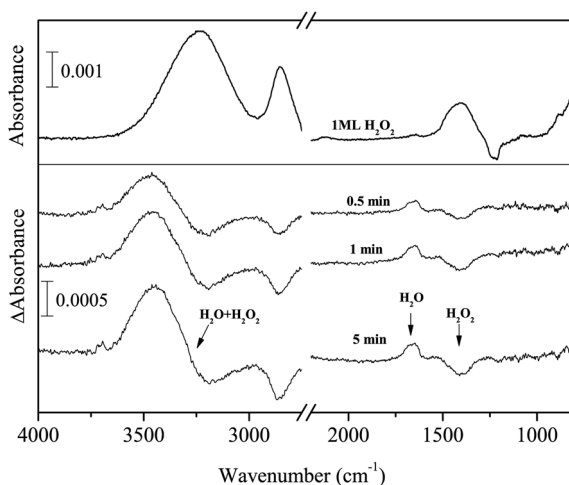


Fig. 8 Variations in the difference spectra of  $H_2O_2$  produced on a- $D_2O$  for up to 5 min at 15 K.



**Table 1** Effective rate constants with statistical errors determined in the present study at 15 K

Reaction	Reaction number	Substrate	Effective rate ( $\text{min}^{-1}$ )	$E_a$ (K) <sup>a</sup>	Reduced mass (u)
$\text{H}_2\text{O}_2 + \text{H}$	3	Al	$7.2 \pm 0.6 \times 10^{-1}$	2508	0.97
		a-D <sub>2</sub> O	$9.9 \pm 0.6 \times 10^{-1}$		
$\text{H}_2\text{O}_2 + \text{D}$	11	Al	$3.2 \pm 0.1 \times 10^{-2}$	2355	1.89
		a-D <sub>2</sub> O	$4.0 \pm 0.6 \times 10^{-2}$		
$\text{D}_2\text{O}_2 + \text{H}$	13	Al	$8.9 \pm 1.1 \times 10^{-1}$	2540	0.97
		a-D <sub>2</sub> O	$9.2 \pm 0.6 \times 10^{-1}$		
$\text{D}_2\text{O}_2 + \text{D}$	7	Al	$2.3 \pm 0.2 \times 10^{-2}$	2384	1.89
		a-D <sub>2</sub> O	$2.2 \pm 0.8 \times 10^{-2}$		

<sup>a</sup> Taquet *et al.*<sup>40</sup>

The column densities of H<sub>2</sub>O formed on the Al and a-D<sub>2</sub>O by reaction (3) were calculated using the band strength of the OH-bending at  $1635 \text{ cm}^{-1}$  ( $1.2 \times 10^{-17} \text{ cm molecule}^{-1}$ ).<sup>28</sup> We determined that the H<sub>2</sub>O yield on a-D<sub>2</sub>O was approximately two orders of magnitude larger than that on the Al at the same H fluence, although the amount of H<sub>2</sub>O<sub>2</sub> consumption on H atom exposure was identical for a-D<sub>2</sub>O and Al (Figure 9).

### Temperature dependence of reaction kinetics

Reaction (3) was studied using pure H<sub>2</sub>O<sub>2</sub> at 10, 20, and 30 K as well as at 15 K. Reaction (3) occurred at all temperatures. We obtained kinetic parameters for reaction (3) ( $k_3'$ ) at each temperature following the procedures described above. Figure 10 shows variations in the relative abundance of pure H<sub>2</sub>O<sub>2</sub> after H atom exposure at 10–30 K. The temperature dependence shows that the saturation value of H<sub>2</sub>O<sub>2</sub> becomes larger with increasing temperature up to 20 K; however, at

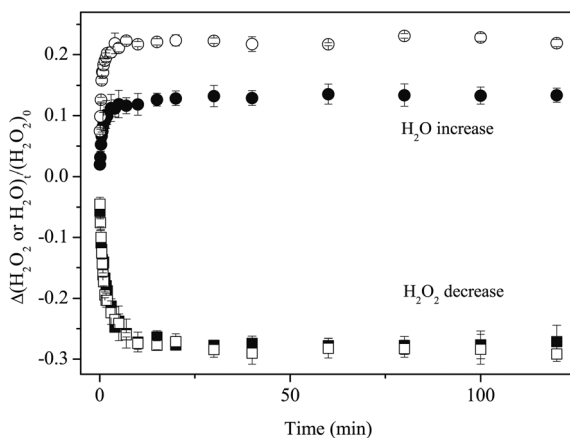


**Fig. 9** Variations in the column densities of H<sub>2</sub>O (circle) and H<sub>2</sub>O<sub>2</sub> (square) normalized to the initial H<sub>2</sub>O<sub>2</sub> amount obtained after H atom exposure to H<sub>2</sub>O<sub>2</sub> at 15 K. Open and filled symbols represent experimental results on a-D<sub>2</sub>O and Al substrate, respectively.



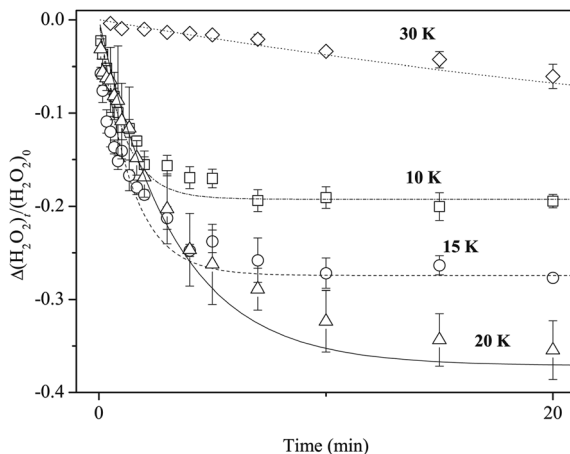


Fig. 10 Variations in the column density of pure  $\text{H}_2\text{O}_2$  normalized to the initial amount after exposure to H atoms at 10 (square), 15 (circle), 20 (triangle), and 30 (diamond) K. Lines are single-exponential decay fits to the plots.

30 K, the reaction is very slow and the saturation value is much less than that below 20 K. The effective rate constant is the largest at 10 K and decreases with increasing temperature. These features were also obtained for reactions on a- $\text{D}_2\text{O}$  ice (Figure 11).

## Discussion

### Quantum tunneling and isotope effect

The reaction of  $\text{H}_2\text{O}_2$  with H atoms and that of their deuterated counterparts has a large activation barrier ( $>2000$  K) in the gas phase.<sup>9,40,41</sup> Therefore, these reactions are expected to proceed through quantum tunneling at 10–30 K even on the

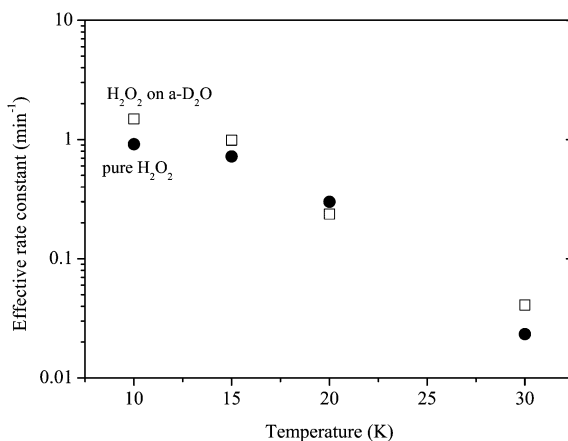


Fig. 11 Temperature dependence of the effective rate constant for reaction (3): filled circle and open square symbols represent the rate for pure  $\text{H}_2\text{O}_2$  and  $\text{H}_2\text{O}_2$  on a- $\text{D}_2\text{O}$ , respectively.



surface, as mentioned earlier. A tunneling reaction strongly depends on the transmission mass of the activation barrier of reaction, as can be seen in equation (4). Theoretical studies proposed that H<sub>2</sub>O formation by reaction (3) initiates from the formation of an intermediate by H atom addition to one O atom in H<sub>2</sub>O<sub>2</sub>, followed by the cleavage of the O–O bond.<sup>9,41</sup> In general, the tunneling mass in the two-body addition reaction is described by the reduced mass  $\mu$ .<sup>12,13</sup> As shown in Table 1, the mass dependence of the reaction rate is evident; the lighter mass results in a faster reaction rate. Thus, we conclude that the reactions of H<sub>2</sub>O<sub>2</sub>/D<sub>2</sub>O<sub>2</sub> with H/D atoms proceed by quantum tunneling.

The ratios of the effective rate constants between reactions (3) and (11) ( $k_3'/k_{11}'$ ) are 23 and 25 for pure H<sub>2</sub>O<sub>2</sub> and H<sub>2</sub>O<sub>2</sub> on a-D<sub>2</sub>O, respectively. Since the effective rate constant  $k_n'$  is expressed as  $k_n[X]$  where X = H or D, the ratio of the effective rate constants is not equal to the ratio of the actual reaction rate constants if [H]  $\neq$  [D]. Assuming that the value of [X] has a linear correlation with the flux of X atoms in the present experiment, the ratios of  $k_3$  to  $k_{11}$  ( $k_3/k_{11}$ ) become 44 and 48 for pure H<sub>2</sub>O<sub>2</sub> and H<sub>2</sub>O<sub>2</sub> on a-D<sub>2</sub>O, respectively, because the D atom flux is approximately twice that of the H atom flux. Similarly, the  $k_{13}/k_7$  ratio was calculated to be 75 and 81 for pure D<sub>2</sub>O<sub>2</sub> and D<sub>2</sub>O<sub>2</sub> on a-D<sub>2</sub>O, respectively. Taquet *et al.*<sup>40</sup> calculated a tunneling probability  $P_n$  through an Eckart potential barrier for reaction (n). In the present study, if we compare the  $P_3/P_{11}$  ratio with the  $k_3/k_{11}$  and the  $P_{13}/P_7$  ratio with the  $k_{13}/k_7$ , we obtain  $k_3/k_{11} \sim 2 \times P_3/P_{11}$  and  $k_{13}/k_7 \sim 3 \times P_{13}/P_7$ . These differences are not surprising because the tunneling probability is significantly affected by the shape of the potential barrier, and it is very difficult to determine the tunneling rate with an accurate barrier for surface reactions. In fact, Taquet *et al.*<sup>40</sup> noted that, although the Eckart model provides a significant improvement over square barriers, which were typically used for this type of calculation, the tunneling probabilities of some reactions at low temperatures can be underestimated (or overestimated).

We obtained the  $k_3/k_7$  ratios of 61 and 88 for pure H<sub>2</sub>O<sub>2</sub>/D<sub>2</sub>O<sub>2</sub> and H<sub>2</sub>O<sub>2</sub>/D<sub>2</sub>O<sub>2</sub> on a-D<sub>2</sub>O, respectively. These values are about one order of magnitude larger than those reported by Miyauchi *et al.*, who determined the  $k_3'/k_7'$  ratio to be 8 in their O<sub>2</sub> hydrogenation/deuteration experiments at 10 K. Since the flux of H atoms was the same with that of D atoms in the previous experiment,<sup>15</sup> the  $k_3'/k_7'$  ratio is certainly equal to the  $k_3/k_7$  ratio on the assumption that the ratio of surface number densities between H and D atoms is same as that of the fluxes. The large difference may arise for several reasons. First, multi-parameter fittings may cause significant errors of  $k_3$  and  $k_7$  in their work. Second, H<sub>2</sub>O and D<sub>2</sub>O would form in O<sub>2</sub> hydrogenation/deuteration *via* separate pathways: OH + OH  $\rightarrow$  H<sub>2</sub>O + O and OD + OD  $\rightarrow$  D<sub>2</sub>O + O, respectively, which are both barrierless reactions. This would lead to an overestimation of the  $k_3/k_7$  ratio. In the present study, these uncertainties are removed because H<sub>2</sub>O<sub>2</sub> or D<sub>2</sub>O<sub>2</sub> are used as the initial reactants. Thus, we believe that our calculated value of  $k_3/k_7$  is more reliable than that obtained in O<sub>2</sub> hydrogenation/deuteration experiments.

Next, we compare the rates of reactions (3) and (5). The  $k_5/k_3$  ratio in the O<sub>2</sub> hydrogenation experiment was reported to be 3.3.<sup>15</sup> Based on the fact that reaction (5) is barrierless and reaction (3) has a large barrier (>2000 K),<sup>9</sup> the value obtained by Miyauchi *et al.* seems to be rather small. Subsequently, we calculated the  $k_5/k_3$  ratio using  $k_3'$  obtained in the present study. The value of  $k_5'$  reported by Miyauchi *et al.* (12.8 min<sup>-1</sup>)<sup>15</sup> was not used for this calculation



because their conditions such as atom fluxes and sample amounts were significantly different from ours. Instead, we used the value of  $k_5'$  ( $5.2 \text{ min}^{-1}$ ) obtained in the following experiment: solid  $\text{O}_2$  ( $\sim 3 \text{ ML}$ ) on an amorphous  $\text{D}_2\text{O}$  ice ( $30 \text{ ML}$ ) was exposed to H atoms (flux:  $2 \times 10^{14} \text{ atoms cm}^{-2} \text{ s}^{-1}$ ) at  $10 \text{ K}$ .<sup>42</sup> After the correction of the flux difference, we obtained the  $k_5/k_3$  ratio of  $\sim 15$ , which is approximately five times larger than that reported by Miyauchi *et al.*<sup>15</sup> Although the sample compositions and the fluxes of H atoms in these two experiments do not exactly match, we believe that the present result would better represent the  $k_5/k_3$  ratio compared to previous studies.

Notably, the observed isotope effect in the hydrogen/deuterium addition to  $\text{H}_2\text{O}_2$  ( $k_3/k_{11}$ ) is much larger than that for one of the astrochemically-important tunneling surface reactions: the hydrogenation/deuteration of CO. Hidaka *et al.*<sup>27</sup> reported that the rate of CO hydrogenation ( $k_{\text{H}}$ ) was larger than CO deuteration ( $k_{\text{D}}$ ), with a  $k_{\text{H}}/k_{\text{D}}$  ratio of 12.5. This isotope effect is approximately four times smaller than that of the hydrogenation/deuteration of  $\text{H}_2\text{O}_2$  observed in the present study. This large difference is rather surprising because the barrier height for the hydrogenation/deuteration of  $\text{H}_2\text{O}_2$  is similar to that of CO.<sup>40,43</sup> We believe that the difference might have been due to accumulation of multiple factors such as differences in residence time of H/D atoms on  $\text{H}_2\text{O}_2$  and CO and the shape of the potential barriers.

As mentioned previously, we assume that the surface density of H atoms is the same as that of D atoms when the flux is equal. However, in a series of experiments under high H and D flux conditions, this may not always be true. Even under the same flux conditions for H and D atoms, the surface density of D atoms ( $[\text{D}]$ ) may become larger than that of H atoms ( $[\text{H}]$ ). Since H atoms can diffuse faster on the surface than D atoms, the recombination probability for H atoms is higher than that for D atoms,<sup>12</sup> resulting in a lower value of  $[\text{H}]$  than that of  $[\text{D}]$  even under the same fluxes. In that case, the ratio of  $[\text{H}]/[\text{D}]$  becomes smaller than 0.5, yielding larger values of  $k_3/k_{11}$  and  $k_{13}/k_7$  than those reported in the present study. Further studies related to the surface densities of H and D atoms are necessary.

### Dependence of reaction efficiency on temperature and type of substrate

The effective rate constants for reaction (3) decrease with increasing substrate temperature (Figure 11). This is opposite to the typical Arrhenius-type behavior where the reaction rate has a positive correlation with temperature. In addition, because reaction (3) occurred through quantum tunneling, the reaction rate should have lesser dependence on the surface temperatures. The decrease of the effective rate can be explained well by the decrease in the number density of H atoms on the surface with increasing temperature because the effective rate  $k_3'$  is expressed by  $k_3[\text{H}]$ . This trend was also observed in CO hydrogenation and deuteration,  $\text{H}_2\text{CO}$  hydrogenation, H–D substitution of  $\text{CH}_3\text{OH}$ , and  $\text{O}_2$  hydrogenation on low-temperature surfaces.<sup>11,42</sup>

The difference of the effective rate constant between reactions of pure  $\text{H}_2\text{O}_2$  and  $\text{H}_2\text{O}_2$  on a- $\text{D}_2\text{O}$  is the largest at  $10 \text{ K}$  and decreases with increasing temperature (Figure 11). The large difference observed at lower temperatures ( $< 15 \text{ K}$ ) may be explained by the difference in the number density of H atoms on the surface because a- $\text{D}_2\text{O}$  would have a much larger surface area compared to planar Al



substrate, as reported for CO hydrogenation by Hidaka *et al.*<sup>44</sup> who determined that the surface area for a-H<sub>2</sub>O with thickness equivalent to  $\sim 17$  ML is approximately nine times larger than that for crystalline H<sub>2</sub>O. In contrast, at elevated temperatures where the residence time of H atoms on the surface is very short even on a-D<sub>2</sub>O, the difference could little be affected by the density of H atoms, which can lead to similar effective rate constant values under both conditions (Figure 11).

In Figure 9, H<sub>2</sub>O yield for the sample of pure H<sub>2</sub>O<sub>2</sub> on Al substrate is lower than that for H<sub>2</sub>O<sub>2</sub> on a-D<sub>2</sub>O, although the decrease of H<sub>2</sub>O<sub>2</sub> is approximately the same for both samples. This difference may be partly explained by immediate desorption of H<sub>2</sub>O formed as a product at the reaction preferentially occurred on the Al substrate. This behavior is also observed in O<sub>2</sub> + D experiments on amorphous silicates and a-H<sub>2</sub>O, where the yield of D<sub>2</sub>O is higher for reactions on a-H<sub>2</sub>O.<sup>39</sup> The heat of reaction (3) ( $285 \text{ kJ mol}^{-1} = 2.9 \text{ eV}$ ) is partly partitioned to the reaction product H<sub>2</sub>O and OH. This energy would be sufficient for H<sub>2</sub>O to desorb from the substrate (Al or a-D<sub>2</sub>O). For the H<sub>2</sub>O<sub>2</sub> on a-D<sub>2</sub>O sample, interaction of H<sub>2</sub>O<sub>2</sub> and H<sub>2</sub>O product with the a-D<sub>2</sub>O surface is much stronger than that with the Al surface because of hydrogen bonding. Therefore, the reaction heat can dissipate into a-D<sub>2</sub>O more easily, and desorption at the reaction surface may be reduced. Furthermore, since a-D<sub>2</sub>O has a large surface area because of pores and cracks, the desorbed H<sub>2</sub>O can be retrapped on the surface of a-D<sub>2</sub>O. This type of H<sub>2</sub>O relaxation and trap has been demonstrated both experimentally<sup>45–47</sup> and theoretically<sup>48,49</sup> to occur during the photodesorption of H<sub>2</sub>O from bulk a-H<sub>2</sub>O. In addition to H<sub>2</sub>O, OH should also form by reaction (3) and can be the source of another H<sub>2</sub>O formation. Accordingly, H<sub>2</sub>O and OH trapped on the surface of a-D<sub>2</sub>O may explain the larger column density of the formed H<sub>2</sub>O than that on the Al substrate (Figure 9).

As shown in Figure 1, solid H<sub>2</sub>O<sub>2</sub> produced on the Al substrate has representative strong absorptions at three positions: 1385 ( $\nu_2$ ), 2827 ( $\nu_2 + \nu_6$ ), and 3326  $\text{cm}^{-1}$  ( $\nu_1$ ).<sup>33</sup> Similarly, for solid H<sub>2</sub>O<sub>2</sub> on a-D<sub>2</sub>O, these three peaks are slightly shifted on the spectrum at 1392, 2852, and 3233  $\text{cm}^{-1}$  (Figure 8). The difference in the peak position for each band is not very large ( $< 25 \text{ cm}^{-1}$ ). However, the peak area of the  $\nu_2 + \nu_6$  combination band was larger by a factor of two for the sample on a-D<sub>2</sub>O, although the peak area of other bands ( $\nu_1$  and  $\nu_2$ ) was identical on both substrates. A relatively strong peak at  $\sim 2850 \text{ cm}^{-1}$  for solid H<sub>2</sub>O<sub>2</sub> is typically assigned to the  $\nu_2 + \nu_6$  combination band;<sup>33,50</sup> however, some studies considered that this assignment is disputable.<sup>51,52</sup> Ignatov *et al.*<sup>51</sup> proposed that this peak is attributable to an OH valence band of the H<sub>2</sub>O<sub>2</sub> molecule placed in the unusual surface environment. The present results imply that the peak intensity at  $\sim 2850 \text{ cm}^{-1}$  might correlate with the configuration of H<sub>2</sub>O<sub>2</sub> on the substrate. In addition, the fact that H<sub>2</sub>O<sub>2</sub> forms hydrogen bonds more on a-D<sub>2</sub>O than on Al could result in the different IR features at  $\sim 2850 \text{ cm}^{-1}$ . In other words, the number of hydrogen bonds between H<sub>2</sub>O<sub>2</sub> and surrounding H<sub>2</sub>O may constrain the peak intensity at  $\sim 2850 \text{ cm}^{-1}$ . If this is the case, it could explain the contradictory behavior of the peak intensity after exposure to atoms (*e.g.* Figures 2 and 8). More detailed experimental and theoretical studies are necessary for the precise peak assignment. Thus, we propose that care should be taken when this IR peak is used for quantification of solid H<sub>2</sub>O<sub>2</sub> in various environments.



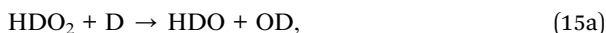
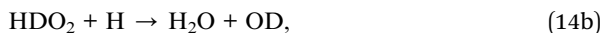
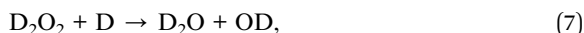
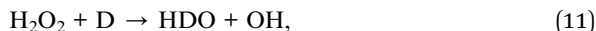
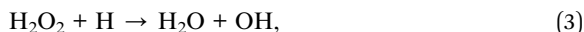
**Dangling OH (OD) bands of reaction products**

We confirmed that the formed solid H<sub>2</sub>O and its isotopologues (HDO and D<sub>2</sub>O) show the dangling OH (OD) bands (*e.g.*, Figure 2). The presence of dangling OH bands in the IR spectrum of solid H<sub>2</sub>O typically indicates that it is amorphous and has a microporous structure.<sup>34</sup> However, we have reported that dangling OH bands are not observed in solid H<sub>2</sub>O formed by codeposition of O<sub>2</sub> and H atoms at 10 K and that the formed ice is amorphous but has a compact structure.<sup>31</sup> These different results suggest that the formed ice structure depends on experimental conditions and that the properties of the reaction products are strikingly different between each study (multilayers with O<sub>2</sub> contaminants *vs.* very thin layers with little contaminants).

**Astrophysical implication**

Deuterated water (HDO and D<sub>2</sub>O) has been identified in the gas phase with HDO/H<sub>2</sub>O and D<sub>2</sub>O/H<sub>2</sub>O ratios up to the order of 10<sup>-2</sup> and 10<sup>-3</sup>, respectively, toward protostars.<sup>53-57</sup> In contrast, deuterated water was not clearly identified in the solid phase; only the upper limit of HDO was determined (HDO/H<sub>2</sub>O < 0.2%–2%).<sup>58,59</sup> Despite the detection of deuterated water in the gas phase only, it is reasonable to consider that deuterated water is also produced by surface reactions on interstellar grains at very low temperatures.

The following reactions are possible to yield water isotopologues from H<sub>2</sub>O<sub>2</sub> and its isotopologues:



We did not study reactions (14) and (15) because of difficulty in producing high-purity HDO<sub>2</sub>. Two types of reaction products are possible for reactions (14) and (15). Since the reduced mass of a reaction to produce the intermediate does not depend on the type of products, we expect that reactions (14a) and (14b) occur to the same extent statistically. In fact, the tunneling probability for reaction (14a) is calculated to be identical with that of reaction (14b).<sup>40</sup> The same is true for reactions (15a) and (15b). Thus, for simplicity, we made a rough assumption based on the obtained results that H atom addition reactions such as reactions (3) and (13) occur faster by a factor of 50 than D atom addition reactions such as reactions (7) and (11). In addition, we assume that the atomic D/H ratio is



constant and the surface diffusion rates of H and D atoms are the same. Under these assumptions, we determined that the HDO/H<sub>2</sub>O ratio was almost identical to the atomic D/H ratio, while the D<sub>2</sub>O formation was negligible ( $\sim 10^{-6}$  that of H<sub>2</sub>O). On the other hand, assuming no isotope effect on the reactions, the HDO/H<sub>2</sub>O ratio becomes twice as large as the atomic D/H ratio; thus, quantum tunneling would cause a decrease of the HDO/H<sub>2</sub>O ratio in this reaction pathway. In other words, if quantum tunneling corrections are not included in a chemical model, the obtained result should overestimate the value of the HDO/H<sub>2</sub>O ratio.

We extend this discussion to other water formation pathways, *i.e.*, reactions (1) (OH + H → H<sub>2</sub>O) and (2) (OH + H<sub>2</sub> → H<sub>2</sub>O + H). For reaction (2), we have experimentally determined the relative efficiency of reactions for all possible isotopologues;<sup>14</sup> H atom abstraction reactions are approximately ten times more efficient than D atom abstraction reactions. Assuming that OH and OD are formed by surface reactions O + H and O + D, respectively, HD/H<sub>2</sub> ratio is 10<sup>-5</sup>, and no D<sub>2</sub> is present, the HDO/H<sub>2</sub>O ratio was very much consistent with the atomic D/H ratio.

In contrast to the former two reaction pathways, the reactions of OH or OD with H or D atoms do not have an activation barrier. Thus, the product ratio would strongly depend on the atomic D/H ratio. Since there are two possible reactions to yield HDO (OH + D → HDO and OD + H → HDO), statistically the HDO/H<sub>2</sub>O ratio is twice as large as the atomic D/H ratio. With regard to the formation of D<sub>2</sub>O, this reaction pathway is the most favorable among the three reaction pathways; the D<sub>2</sub>O/H<sub>2</sub>O ratio is statistically the square of the value of the D/H ratio. For example, the D<sub>2</sub>O/H<sub>2</sub>O ratio is 10<sup>-4</sup> if the atomic D/H is 10<sup>-2</sup>. This value is two to four orders of magnitude higher than that estimated by other pathways under the same assumptions. Therefore, the OD + D reaction is the only possible pathway to effectively yield D<sub>2</sub>O in MCs.

Moreover, it is important to note that, on grain surfaces, the deuterium fractionation of water occurs only during the formation by surface reactions at the typical temperature of MCs ( $\sim 10$  K). This is supported by the fact that H<sub>2</sub>O does not react with D atoms at  $< 15$  K<sup>60</sup> and thermal H–D exchange does not occur at  $< 100$  K,<sup>61</sup> which prevents the D-enrichment by H–D substitution with other deuterium-enriched species after the formation of H<sub>2</sub>O on the grains. The reactivity of water with D atoms at low temperatures differs from that of organic species such as CH<sub>3</sub>OH,<sup>25,60</sup> H<sub>2</sub>CO,<sup>13,27</sup> and CH<sub>3</sub>NH<sub>2</sub><sup>62</sup> where H–D exchange occurs for these molecules by reacting with D atoms at temperatures as low as 10 K.

Based on the present and previous experimental results for water formation, we suggest that the HDO/H<sub>2</sub>O ratio might be a key parameter to estimate the atomic D/H ratio during the formation of water. Namely, the following relationship is roughly derived from experimental studies:  $(D/H)_{\text{atom}} \leq (HDO/H_2O) \leq 2(D/H)_{\text{atom}}$  or  $1/2(HDO/H_2O) \leq (D/H)_{\text{atom}} \leq (HDO/H_2O)$ , where  $(D/H)_{\text{atom}}$  and  $(HDO/H_2O)$  represent the atomic D/H on grains and the HDO/H<sub>2</sub>O ratio formed by surface reactions, respectively. Note that these relationships were derived with reference to experimental studies for surface reactions. In addition to surface reactions, deuterium fractionation of water by gas phase reactions may also be possible.<sup>63</sup> Moreover, energetic processes induced by UV and cosmic rays might cause hydrogen isotopic fractionation of water during its decomposition and interactions with other ice components, both of which may modify the HDO/H<sub>2</sub>O ratio. Therefore, we propose that further collaborative theoretical and



experimental studies on surface and gas phase chemistries are necessary to construct a complete chemical model regarding the evolution of the water D/H ratio in MCs.

## Acknowledgements

The authors thank Drs H. Hidaka and T. Hama for fruitful discussions at the earlier stages of manuscript preparation. We also thank an anonymous referee for providing constructive comments. This work is partly supported by a Grant-in-Aid for Scientific Research from the Japan Society for the Promotion of Science. Y.O. has received funding from the Kurita Water and Environment Foundation.

## References

- 1 E. Herbst and W. Klemperer, *Astrophys. J.*, 1973, **185**, 505–533.
- 2 T. I. Hasegawa, E. Herbst and C. M. Leung, *Astrophys. J. Suppl.*, 1992, **82**, 167–195.
- 3 A. Tielens and W. Hagen, *Astron. Astrophys.*, 1982, **114**, 245–260.
- 4 F. Dulieu, L. Amiaud, E. Congiu, J. H. Fillion, E. Matar, A. Momeni, V. Pirronello and J. L. Lemaire, *Astron. Astrophys.*, 2010, **512**, 5.
- 5 K. Hiraoka, T. Miyagoshi, T. Takayama, K. Yamamoto and Y. Kihara, *Astrophys. J.*, 1998, **498**, 710–715.
- 6 D. P. Jing, J. He, M. Bonini, J. R. Brucato and G. Vidali, *J. Phys. Chem. A*, 2013, **117**, 3009–3016.
- 7 D. P. Jing, J. He, J. Brucato, A. De Sio, L. Tozzetti and G. Vidali, *Astrophys. J.*, 2011, **741**, 5.
- 8 R. Atkinson, D. L. Baulch, R. A. Cox, J. N. Crowley, R. F. Hampson, R. G. Hynes, M. E. Jenkin, M. J. Rossi and J. Troe, *Atmos. Chem. Phys.*, 2004, **4**, 1461–1738.
- 9 H. Koussa, M. Bahri, N. Jaidane and Z. Ben Lakhdar, *THEOCHEM*, 2006, **770**, 149–156.
- 10 H. M. Cuppen and E. Herbst, *Astrophys. J.*, 2007, **668**, 294–309.
- 11 N. Watanabe and A. Kouchi, *Prog. Surf. Sci.*, 2008, **83**, 439–489.
- 12 T. Hama and N. Watanabe, *Chem. Rev.*, 2013, **113**, 8783–8839.
- 13 H. Hidaka, M. Watanabe, A. Kouchi and N. Watanabe, *Astrophys. J.*, 2009, **702**, 291–300.
- 14 Y. Oba, N. Watanabe, T. Hama, K. Kuwahata, H. Hidaka and A. Kouchi, *Astrophys. J.*, 2012, 749.
- 15 N. Miyauchi, H. Hidaka, T. Chigai, A. Nagaoka, N. Watanabe and A. Kouchi, *Chem. Phys. Lett.*, 2008, **456**, 27–30.
- 16 H. M. Cuppen, S. Ioppolo, C. Romanzin and H. Linnartz, *Phys. Chem. Chem. Phys.*, 2010, **12**, 12077–12088.
- 17 Y. Oba, N. Watanabe, A. Kouchi, T. Hama and V. Pirronello, *Phys. Chem. Chem. Phys.*, 2011, **13**, 15792–15797.
- 18 T. Lamberts, H. M. Cuppen, S. Ioppolo and H. Linnartz, *Phys. Chem. Chem. Phys.*, 2013, **15**, 8287–8302.
- 19 G. W. Fuchs, H. M. Cuppen, S. Ioppolo, C. Romanzin, S. E. Bisschop, S. Andersson, E. F. van Dishoeck and H. Linnartz, *Astron. Astrophys.*, 2009, **505**, 629–639.
- 20 C. Pirim and L. Krim, *Chem. Phys.*, 2011, **380**, 67–76.



- 21 N. Watanabe and A. Kouchi, *Astrophys. J.*, 2002, **571**, L173–L176.
- 22 N. Watanabe, T. Shiraki and A. Kouchi, *Astrophys. J.*, 2003, **588**, L121–L124.
- 23 N. Watanabe, A. Nagaoka, T. Shiraki and A. Kouchi, *Astrophys. J.*, 2004, **616**, 638–642.
- 24 H. Hidaka, N. Watanabe, T. Shiraki, A. Nagaoka and A. Kouchi, *Astrophys. J.*, 2004, **614**, 1124–1131.
- 25 A. Nagaoka, N. Watanabe and A. Kouchi, *J. Phys. Chem. A*, 2007, **111**, 3016–3028.
- 26 N. Watanabe, A. Nagaoka, H. Hidaka, T. Shiraki, T. Chigai and A. Kouchi, *Planet. Space Sci.*, 2006, **54**, 1107–1114.
- 27 H. Hidaka, A. Kouchi and N. Watanabe, *J. Chem. Phys.*, 2007, 126.
- 28 P. A. Gerakines, W. A. Schutte, J. M. Greenberg and E. F. van Dishoeck, *Astron. Astrophys.*, 1995, **296**, 810–818.
- 29 M. J. Loeffler and R. A. Baragiola, *J. Phys. Chem. A*, 2011, **115**, 5324–5328.
- 30 R. G. Smith, S. B. Charnley, Y. J. Pendleton, C. M. Wright, M. M. Maldoni and G. Robinson, *Astrophys. J.*, 2011, **743**, 13.
- 31 Y. Oba, N. Miyauchi, H. Hidaka, T. Chigai, N. Watanabe and A. Kouchi, *Astrophys. J.*, 2009, **701**, 464–470.
- 32 S. Ioppolo, H. M. Cuppen, C. Romanzin, E. F. van Dishoeck and H. Linnartz, *Astrophys. J.*, 2008, **686**, 1474–1479.
- 33 J. A. Lannon, F. D. Verderam and R. W. Anderson, *J. Chem. Phys.*, 1971, **54**, 2212–2223.
- 34 V. Buch and J. P. Devlin, *J. Chem. Phys.*, 1991, **94**, 4091–4092.
- 35 J. P. Devlin, *J. Mol. Struct.*, 1990, **224**, 33–43.
- 36 D. F. Hornig, H. F. White and F. P. Reding, *Spectrochim. Acta*, 1958, **12**, 338–349.
- 37 J. P. Devlin, *J. Chem. Phys.*, 2000, **112**, 5527–5529.
- 38 R. T. Garrod, V. Wakelam and E. Herbst, *Astron. Astrophys.*, 2007, **467**, 1103–1115.
- 39 H. Chaabouni, M. Minissale, G. Manico, E. Congiu, J. A. Noble, S. Baouche, M. Accolla, J. L. Lemaire, V. Pirronello and F. Dulieu, *J. Chem. Phys.*, 2012, **137**, 234706.
- 40 V. Taquet, P. S. Peters, C. Kahane, C. Ceccarelli, A. Lopez-Sepulcre, C. Toubin, D. Duflot and L. Wiesenfeld, *Astron. Astrophys.*, 2013, **550**, 23.
- 41 B. A. Ellingson, D. P. Theis, O. Tishchenko, J. Zheng and D. G. Truhlar, *J. Phys. Chem. A*, 2007, **111**, 13554–13566.
- 42 Y. Oba, N. Miyauchi, T. Chigai, H. Hidaka, N. Watanabe and A. Kouchi, in *Physics and Chemistry of Ice 2010*, Hokkaido University Press, 2011, Y. Furukawa, G. Sazaki, T. Uchida, and N. Watanabe, Eds., 361–368.
- 43 D. E. Woon, *Astrophys. J.*, 2002, **569**, 541–548.
- 44 H. Hidaka, N. Miyauchi, A. Kouchi and N. Watanabe, *Chem. Phys. Lett.*, 2008, **456**, 36–40.
- 45 T. Hama, M. Yokoyama, A. Yabushita, M. Kawasaki, S. Andersson, C. M. Western, M. N. R. Ashfold, R. N. Dixon and N. Watanabe, *J. Chem. Phys.*, 2010, **132**, 8.
- 46 A. Yabushita, T. Hama, M. Yokoyama, M. Kawasaki, S. Andersson, R. N. Dixon, M. N. R. Ashfold and N. Watanabe, *Astrophys. J.*, 2009, **699**, L80–L83.
- 47 K. I. Oberg, H. Linnartz, R. Visser and E. F. van Dishoeck, *Astrophys. J.*, 2009, **693**, 1209–1218.



- 48 S. Andersson and E. F. van Dishoeck, *Astron. Astrophys.*, 2008, **491**, 907–916.
- 49 C. Arasa, S. Andersson, H. M. Cuppen, E. F. van Dishoeck and G. J. Kroes, *J. Chem. Phys.*, 2010, **132**, 12.
- 50 A. Engdahl, B. Nelander and G. Karlstrom, *J. Phys. Chem. A*, 2001, **105**, 8393–8398.
- 51 S. K. Ignatov, A. G. Razuvaev, P. G. Sennikov and O. Schrems, *THEOCHEM*, 2009, **908**, 47–54.
- 52 P. G. Sennikov, S. K. Ignatov and O. Schrems, *ChemPhysChem*, 2005, **6**, 392–412.
- 53 H. M. Butner, S. B. Charnley, C. Ceccarelli, S. D. Rodgers, J. R. Pardo, B. Parise, J. Cernicharo and G. R. Davis, *Astrophys. J.*, 2007, **659**, L137–L140.
- 54 C. Ceccarelli, C. Dominik, E. Caux, B. Lefloch and P. Caselli, *Astrophys. J.*, 2005, **631**, L81–L84.
- 55 A. Coutens, C. Vastel, E. Caux, C. Ceccarelli, S. Bottinelli, L. Wiesenfeld, A. Faure, Y. Scribano and C. Kahane, *Astron. Astrophys.*, 2012, **539**, 12.
- 56 B. Parise, E. Caux, A. Castets, C. Ceccarelli, L. Loinard, A. Tielens, A. Bacmann, S. Cazaux, C. Comito, F. Helmich, C. Kahane, P. Schilke, E. van Dishoeck, V. Wakelam and A. Walters, *Astron. Astrophys.*, 2005, **431**, 547–554.
- 57 C. Vastel, C. Ceccarelli, E. Caux, A. Coutens, J. Cernicharo, S. Bottinelli, K. Demyk, A. Faure, L. Wiesenfeld, Y. Scribano, A. Bacmann, P. Hily-Blant, S. Maret, A. Walters, E. A. Bergin, G. A. Blake, A. Castets, N. Crimier, C. Dominik, P. Encrenaz, M. Gerin, P. Hennebelle, C. Kahane, A. Klotz, G. Melnick, L. Paganì, B. Parise, P. Schilke, V. Wakelam, A. Baudry, T. Bell, M. Benedettini, A. Boogert, S. Cabrit, P. Caselli, C. Codella, C. Comito, E. Falgarone, A. Fuente, P. F. Goldsmith, F. Helmich, T. Henning, E. Herbst, T. Jacq, M. Kama, W. Langer, B. Lefloch, D. Lis, S. Lord, A. Lorenzani, D. Neufeld, B. Nisini, S. Pacheco, J. Pearson, T. Phillips, M. Salez, P. Saraceno, K. Schuster, X. Tielens, F. van der Tak, M. H. D. van der Wiel, S. Viti, F. Wyrowski, H. Yorke, P. Cais, J. M. Krieg, M. Olberg and L. Ravera, *Astron. Astrophys.*, 2010, **521**, 5.
- 58 E. Dartois, W. F. Thi, T. R. Geballe, D. Deboffle, L. d'Hendecourt and E. van Dishoeck, *Astron. Astrophys.*, 2003, **399**, 1009–1020.
- 59 B. Parise, T. Simon, E. Caux, E. Dartois, C. Ceccarelli, J. Rayner and A. Tielens, *Astron. Astrophys.*, 2003, **410**, 897–904.
- 60 A. Nagaoka, N. Watanabe and A. Kouchi, *Astrophys. J.*, 2005, **624**, L29–L32.
- 61 J. P. Devlin and V. Buch, *J. Chem. Phys.*, 2007, **127**, 4.
- 62 Y. Oba, T. Chigai, Y. Osamura, N. Watanabe and A. Kouchi, *Meteorit. Planet. Sci.*, 2014, **49**, 117–132.
- 63 H. Roberts, E. Herbst and T. J. Millar, *Astron. Astrophys.*, 2004, **424**, 905–917.

